Chapter 3

Zirconia-Related Phases in the Zirconia/Titanium Diffusion Couple after Annealing at 1100° to 1550°C

3.1 Introduction

Extensive research[1-3] has been performed on the reactions between the titanium and the zirconia (ZrO_2), mostly using microhardness measurements, metallographic, and x-ray diffraction (XRD) analyses. Economos and Kingery[1] indicated that titanium penetrated along the grain boundaries of ZrO_2, without the formation of a new phase, other than the black oxygen-deficient zirconia (ZrO_{2-x}). Weber *et al.*[2] discovered limited dissolution of titanium in zirconia as well as the blackening of zirconia, when the melting titanium reacted with the ZrO_2 crucible. Ruh[3] found that up to 4 at.% of titanium were retained at room temperature as a substitutional solid solution in zirconia, while up to approximately 10 mol% zirconia would be dissolved in titanium with zirconium and oxygen entering into the substitutional and interstitial positions of titanium lattice, respectively.

The darkening of yittria-stabilized zirconia were observed at high temperatures under reducing conditions.[4, 5] Moya and his coworkers[6, 7] attributed the darkening of partially stabilized zirconia to the formation of Zr^{+3} ions. Using the electron spin resonance (ESR) method, they claimed that the difference in color should be caused by the ex-solution of impurities, mainly iron, from the bulk to the surface of zirconia polycrystals under reducing conditions. In the other way, other studies found[8, 9] the black color of zirconia followed from the formation of nonstoichiometric ZrO_{2-x}, where *x* indicates the deviation from stoichiometry. Rice[10] stated that the

zirconia was blackened by loss of intrinsic oxygen. Ingo[11] indicated that the change of valence states of zirconium was responsible for darkening of 8wt% yttria-zirconia plasma-sprayed thermal barrier coatings, while the segregation and exsolution of impurities (Fe, Al, Si, and Na) could be ruled out as causes of darkening.

The phase transformation of zirconia have been subjected to comprehensive investigations in the past several decades.[12-20] In a systematic study on 12wt% Y_2O_3-ZrO_2, Chaim *et al.*[21] showed that a tweed-like microstructure existed inside c-ZrO_2, resulting from the strain field of small coherent *t*-ZrO_2 precipitates after sintering at 1600°C/2 h. While a twinned *t'*-ZrO_2 phase with antiphase domain boundaries was observed after a subsequent annealing at 1550°C/1 h and a rapid cooling, twinned *t*-ZrO_2 precipitates (or colonies) among the *c*-ZrO_2 matrix were found after long-term annealing at 1400°C. However, precipitate-free zones at the perimeter of *c*-ZrO_2 grains with fine *t*-ZrO_2 precipitates were observed after annealing at 1250°C. The twinned *t'*-ZrO_2 phase, which resulted from the untransformable *t*-ZrO_2, were featured by a high Y_2O_3 content up to 10 wt% as mentioned in several other previous studies.[17] The twins were able to relieve the strains arising from the small tetragonality of the product phase and the small molar volume change accompanying transformation.

Previous studies[1-3] mentioned above did not deal with the fine features and new phases (except α-Zr) formed in the reaction zone of zirconia and titanium due to the instrumental limitation. Using analytical transmission electron microscopy, Lin and Lin[22] characterized the microstructure abutting the interface of Ti melt and ZrO_2. They reported that the liquid-solid reaction at 1750°C/7 min caused zirconia to transform into oxygen-deficient zirconia (ZrO_{2-x}) with an O/Zr ratio as low as 1.53. While a significant

amount of oxygen accumulated at grain boundaries of titanium, the remainder being dissolved in titanium as α-Ti(O). An ordered titanium suboxide (Ti_3O) was then formed from a solid solution of α-Ti(O) during cooling. Moreover, the twinned α-Zr(O) was excluded from ZrO_{2-x}, leading to the formation of fine crystalline ZrO_{2-x} with a high O/Zr ratio ($\approx$1.9) during cooling. The lamellae of Ti_2ZrO and α-Ti(Zr, O) were also found by TEM/EDS analysis.

In the heat treatment experiments of the ZrO_2/Ti diffusion couple conducted recently by Lin and Lin,[23] the lamellar and the spherical Ti_2ZrO as well as the orthorhombic β'-Ti were found to exist in the titanium side after annealing at 1550°C/30 min. On heating, the dissolution of a large amount of zirconium and oxygen into titanium gave rise to the metastably supersaturated disordered α-Ti(Zr, O) solid solution where Ti_2ZrO subsequently precipitated, while the β-Ti coexisting with α-Ti at high temperatures was transformed to the orthorhombic β'-Ti during cooling. However, the microstructural variation of zirconia in the reaction affected zone has not been studied thoroughly to date. The purpose of the present study is to investigate the phases and microstructure of zirconia in the Ti/ZrO_2 diffusion couple annealed at 1100° to 1550°C for 6 h using scanning electron microscopy (SEM) and transmission electron microscopy (TEM) both attached with an energy-dispersive spectrometer (EDS).

3.2 Experimental Procedures

Bulk ZrO_2 specimens used in this study were prepared from the powder of 3 mol% Y_2O_3 partially stabilized zirconia (> 94wt% ZrO_2+HfO_2, 5.4wt% Y_2O_3, < 0.001wt% Fe_2O_3, <0.01wt% SiO_2, <0.005wt% Na_2O, <0.005wt% TiO_2, <0.02wt% Cl, <0.005wt % SO_4^{2-}; Toyo Soda Mfg. Co., Tokyo, Japan)

by hot-pressing (Model HP50-MTG-7010, Thermal Techno. Inc., Santa Rosa, CA). The specimens were heated to and held at 300°C for 3 min under 5 MPa at a heating rate of 30°C/min, while heating to and being held at 1450°C for 30 min under 30 MPa at a heating rate of 25°C/min. During cooling, pressure was released at 1100°C and then furnace cooled down to room temperature.

The as hot-pressed ZrO_2 and commercially available pure titanium (with a nominal composition of 99.31wt% Ti, 0.25wt% O, 0.01wt% H, 0.03wt% N, 0.10wt% C, 0.30wt% Fe; designated as Cp-Ti hereafter.) were cut and machined to the dimensions of 14 mm x 14 mm x 5 mm. Their surfaces were ground and polished to 0.5 μm using a diamond paste, and then were ultrasonically cleaned in acetone. The Cp-Ti was inserted in between two ZrO_2 specimens to form a sandwiched sample, and then placed in a graphite furnace; it was pressed in a preparatory process at 5 MPa, before the furnace was evacuated to 2×10^{-4} Torr and then filled with argon to a pressure of one atmosphere. This cycle of evacuation and purging was repeated at least three times. The temperature was increased to 1000°C at a rate of 30°C/min, and then to 1100°, 1300°, and 1550°C at 25°C/min, respectively, where the specimen was then held for 6 h. During cooling, the temperature was lowered to room temperature at a rate of 25°C/min and then the pressure was released.

The cross-sectional TEM specimens perpendicular to the interface of zirconia and titanium were cut into pieces of approximately 3 mm x 2 mm x 0.5 mm. They were ground down to ~80 μm thick with a diamond matted disc, polished with the diamond pastes of 6, 3, and 1 μm in sequence, dimpled to 50 μm thick, and finally milled by a precision ion milling (Model 691, Gatan Inc., Pleasanton, CA). The microstructure of the

zirconia side in the reaction affected zone was characterized using a scanning electron microscope (SEM, Model JSM-6330F, JEOL Ltd., Tokyo, Japan) and an analytical transmission electron microscope (TEM, Model JEM 2000Fx, JEOL Ltd., Tokyo, Japan) equipped with an energy-dispersive x-ray spectrometer (EDS, Mode ISIS300, Oxford Instrument Inc., London, UK). The quantitative composition analyses were performed based on the principle of Cliff-Lorimer standardless method.[24]

3.3 Results and Discussion

3.3.1 Annealing at 1100°C

Figure 3.1(a) displays the TEM micrograph of the *t*-ZrO_{2-x} or tetragonal deficient-oxygen zirconia in the ceramic side of the ZrO_2/Ti diffusion couple after reaction at 1100°C/6 h. An average *t*-ZrO_{2-x} particle size of around 0.5 μm is obtained so that no grain growth was noticeable. Figure 3.1(b) shows the diffraction ring pattern of the *t*-ZrO_{2-x}. The first, second, third and fourth rings correspond to the *t*-ZrO_{2-x} {111}, {200}, {112} and {220} planes, respectively. No phases other than the oxygen-deficient zirconia were found in the ceramic side.

3.3.2 Annealing at 1300°C

Figure 3.2 displays an SEM micrograph (backscattered electron image, BEI) of the zirconia side of the ZrO_2/Ti diffusion couple after reaction at 1300°C/6 h. The micrographs reveals the coexistence of α-Zr, labeled as "A" (bright), and *t*-ZrO_{2-x}, labeled as "B" (gray). The mean particle size of both α-Zr and *t*-ZrO_{2-x} were approximately 1 μm. The α-Zr appeared brighter than the ZrO_{2-x} in the BEI due to atomic number effect. Also shown in Fig. 3.2, the dark areas represent voids and a coarsen intergranular α-Zr was arrowed.

Figure 3.3(a) displays the TEM micrograph of α-Zr and *t*-ZrO_{2-x}, corresponding to Fig. 3.2 on the zirconia side of the ZrO_2/Ti diffusion couple after reaction at 1300°C/6 h. The selected area diffraction pattern (SADP) of α-Zr, shown in Fig. 3.3(b), was identified as that of a hexagonal structure with $a \approx 3.18$ Å and $c \approx 5.01$ Å. Figure 3.3(c) shows the EDS spectrum of α-Zr, which reveals a composition of 81.03 at.% Zr, 15.29 at.% O and 3.68 at.% Y. Figure 3.3(d) displays the SADP of t-ZrO_{2-x} on the zone axis of [110] with parameters $a \approx 5.05$ Å and $c \approx 5.14$ Å. Figure 3.3(e) presents the EDS spectrum of *t*-ZrO_{2-x}, consisting of 33.29 at.% Zr, 61.45 at.% O and 5.26 at.% Y corresponding with $ZrO_{1.846}$. It is consistent with that fact that a two-phase region of α-Zr (O) and *t*-ZrO_{2-x} with a wide range of oxygen content (30.8 at.% O-63.5 at.% O) exists in the phase diagram of Zr–O at 1300°C. It also indicates that the solubility of α-Zr in tetragonal ZrO_{2-x} declined as the temperature decreased.[25] Hence, the α-Zr (O) tends to segregated from the supersaturated solid solution of ZrO_{2-x} during cooling, and excluding Zr can increase the O/Zr ratio of the oxygen-deficient zirconia.

3.3.3 Annealing at 1550°C

Figure 3.4(a) shows a backscattered electron image (BEI) at the zirconia side of the ZrO_2/Ti diffusion couple after reaction at 1550°C/6 h. It reveals the coarsening of intergranular α-Zr (marked as "A") and *t*-ZrO_{2-x} (marked as "B") in the *c*-ZrO_{2-x} matrix (marked as "C"). The α-Zr was approximately 10 μm in size. Parts of the α-Zr were easy peeled off to form voids (black) at the grain boundaries of zirconia by mechanical grinding and polishing. The grain size of zirconia matrix was about 50 μm on average, which was much larger than that of the zirconia after reaction at either 1100° or 1300°C.

The high chemical affinity of titanium to oxygen, as well as the high solid solubility of oxygen in titanium (about 14.5%), is the driving force of oxidation-reduction reaction, causing the formation of oxygen-dificient zircona (ZrO_{2-x}) and α-case in titanium (oxygen stabilized α phase). The oxidation-reduction reaction can be demonstrated by the following reaction.

$$O^{x}_{o\,\text{in ZrO}_2} \rightarrow V^{\bullet\bullet}_{o\,\text{in ZrO}_2} + 2e'_{in\,\text{ZrO}_2} + O_{\text{soild solution in Ti}} \quad (1)$$

The oxygen vacancies, resulting from the reduction reaction of ZrO_2 by Ti on annealing, as indicated by Eq. (1), was believed to dominate in present study, even though the equilibrium concentration of oxygen vacancies increases with temperature. It is well known that vacancy is the predominant diffusion mechanism in zirconia and the oxygen vacancies increase with the deviation from stochiometry. Therefore the atoms diffuse more rapidly with decreasing O/Zr ratio because of the reduction reaction of oxygen-deficient zirconia. The grain growth of ZrO_{2-x} during annealing at high temperatures is thus enhanced in that the grain growth is governed by the diffusion phenomenon.

The rate of oxidation-reduction reaction between zirconia and titanium increased with temperature, leading to a significant increase in oxygen vacancies or diffusivity, and an enhanced grain growth of ZrO_{2-x} as well. In contrast, the grain size of as hot-pressed zirconia, which was subjected to the same heat treatment as the zirconia/titanium diffusion couple, was about 2~3 μm in average as show in Fig. 3.4(b). This fact indicates that the reaction between zirconia and titanium played a very important role in grain growth. During cooling, α-Zr was segregated on grain boundaries by the exsolution of zirconium from ZrO_{2-x}. The segregation of α-Zr in the grain

boundaries can suppress further grain growth of ZrO_{2-x} due to the dragging effect. It is evidenced that no intragranular α-Zr was observed in the present study.

Figure 3.5(a) presents the TEM micrograph at the zirconia side of the ZrO_2/Ti diffusion couple after the reaction at 1550°C/6 h. The twinned *t*'-ZrO_{2-x} was embedded in the *t*'-ZrO_{2-x} matrix. Reflections of the type *odd*, *odd*, *even*, forbidden for *c*-ZrO_2, were applied extensively to distinguish the *c*-ZrO_2 from the *t*-ZrO_2 phase. A 〈111〉 zone axis orientation was used since all possible *t*-ZrO_2 variants were identified using {112}-type reflections.[12-20] Figures 3.5(b) and (c) show the microdiffraction patterns of the *t*'-ZrO_{2-x} matrix and the twin *t*'-ZrO_{2-x}, respectively, with the electron beam along the zone axis [111]. The fact that the reflections {112} were absent in Fig. 3.5(b) and (c) indicated that both the matrix and the twin were tetragonal rather than cubic ZrO_{2-x}. These results were basically in agreement with the observations conducted by Heuer *et al.*[16, 17, 21], who described the displacive *c*→*t'* transformation in ZrO_2 alloys.

The ZrO_2 had a high Y_2O_3 content up to more than 10 wt% in previous studies,[16, 21] however, the Y_2O_3 concentration in ZrO_2 was as low as 5.36 wt% (3 mol%) in this study. According to the ZrO_2-Y_2O_3 phase diagram, the ZrO_2 with 3 mol% Y_2O_3 at 1550°C was predominantly tetragonal rather than cubic ZrO_2,[26] indicating that the *c*→*t'* displacive transformation should not have taken place in 3 mol% Y_2O_3-ZrO_2. However, a significant increase in oxygen vacancies, in consequence of the reaction between zirconia and titanium, triggered the stabilization effect of zirconia. Therefore, it was inferred that the zirconia would be in the cubic phase solid solution region during annealing at 1550°C and the *t'* phase was formed as

the diffusion couple was cooled in furnace to room temperature following annealing.

At a position further away from the interface, it was found that lenticular *t*-ZrO_{2-x} with three {100} type of variants precipitated in the *c*-ZrO_{2-x} matrix on the zirconia side after annealing at 1550°C/6 h, as shown in Fig. 3.6(a). It was inferred that the specimen was cooled down from the two-phase (*c* + *t*) region in the ZrO_2-Y_2O_3 phase diagram. On the other hand, the cubic oxygen difficient zirconia would exist at 1550°C, since the eutectoid reaction, as expressed in the following equation, took place at about 1525°C.[27]

$$ZrO_{2-x}(cubic) \leftrightarrow ZrO_{2-x}(tetragonal) + Zr(\alpha) \quad (2)$$

Figure 3.6(b) shows clearly, at a higher magnification, the contrast of the stress field due to the ordering of oxygen in the *c*-ZrO_{2-x} matrix. The EDS spectrum of *c*-ZrO_{2-x}, as shown in Figure 3.6(c), revealed that lenticular *t*-ZrO_{2-x} consisted of 35.5 at.% Zr, 58.48 at.% O and 6.02 at.% Y, corresponding to an oxygen-deficient zirconia of 7.25 mol% Y_2O_3–$ZrO_{1.41}$. The lower limit of the solidus of cubic ZrO_{2-x} phase lies in the range of $1.64 < O/Zr < 1.70$ between 1815° to 2065°C, while that for *t*-ZrO_{2-x} was 1.925 below 1300°C.[27, 28] It was not surprising that the measured O/Zr ratio in the present study was as low as 1.41 because of the vehement oxidation–reduction reaction on annealing and sluggish diffusion during cooling. The SADP's of the *c*-ZrO_{2-x} matrix with the zone axes being [110] and [310]. were shown in Fig. 3.6(d) and (e), respectively. The fact that (112) reflections were absent in Fig. 3.6(d) confirmed that the matrix was c-symmetric in structure. The ordered structure was characterized by

$\frac{1}{5}\{113\}$ superlattice reflections for zirconia unit cell in the mean time.

According to the Ellingham diagram the Ti cannot reduce the ZrO_2. If the following reactions were applicable in the present study:

$$Ti + O_2 \rightarrow TiO_2 \tag{3}$$

$$Zr + O_2 \rightarrow ZrO_2 \tag{4}$$

Then the oxidation-reduction reaction could have been written as follows:

$$ZrO_2 + Ti \rightarrow Zr + TiO_2 \tag{5}$$

The Gibbs free energy for the oxidation-reduction reaction (5) is $\Delta g = \Delta g_{\text{oxid (Ti)}} - \Delta g_{\text{oxid (Zr)}}$, where $\Delta g_{oxid(Ti)}$ and $\Delta g_{oxid(Zr)}$ are the Gibbs free energies of oxidation of Ti and Zr, respectively. Based upon the Ellingham diagram, the Gibbs free energy for the oxidation-reduction reaction (5) Δg is positive, indicating that Ti cannot reduce ZrO_2. However, these are not the cases in the present study. Based on the experimental results, the following dissolution reaction should be applied.

$$1/2O_{2(g)} \rightarrow O''_{i(\text{in titanium})} + 2h^{\bullet}_{(\text{in titanium})} \tag{6}$$

The Gibbs free energy of oxygen dissolution in solid titanium Δg_{diss} is related to the temperature by the following equation.[29]

$$\Delta g_{diss} = -RT \ln K_{diss} = -609 + 0.126T \text{ (KJ/mol)} \tag{7}$$

where K_{diss} is the equilibrium constant of the reaction (6), R the gas constant (≈ 8.3144 J mol^{-1} K^{-1}), and T the absolute temperature. When T = 1550°C = 1823K, $\Delta g_{\text{diss}} = -379.30$ (KJ/mol) . On the other hand, the reduction reaction of zirconia can be expressed as follows.

$$O_{o\ (\text{in zirconia})}^{x} \rightarrow V_{o\ (\text{in zirconia})}^{\bullet\bullet} + 2e'_{(\text{in zirconia})} + 1/2O_{2(g)} \tag{8}$$

The Gibbs free energy of the reduction reaction (8) Δg_{red} can be calculated from the following equation,[30]

$$\Delta g_{red} = -RT \ln K_{red} = -RT\left(2 - \frac{68,000}{T}\right) \tag{9}$$

where K_{red} is the equilibrium constant of the reduction reaction (8), of which the nature logarithm is equal to (2 − 68,000/T). When T = 1550°C = 1823K, $\Delta g_{red} = 0.54$(KJ/mol) . The resultant reaction of the reactions (6) and (8) is written by the following equation:

$$O_{O\ (\text{in zirconia})}^{X} \rightarrow V_{O\ (\text{in zirconia})}^{\bullet\bullet} + 2e'_{\ (\text{in zirconia})} + O_{i\ (\text{in titanium})}^{''} + 2h^{\bullet}_{\ (\text{in titanium})} \tag{10}$$

Since $\Delta g = \Delta g_{\text{red}} + \Delta g_{\text{diss}} = 0.54 - 379.30 = -378.76$(KJ/mol) at 1550°C, the reaction (10) is thermodynamically favorable consistent with the results observed in the present study.

3.3.4 Proposed model of phase development at 1300 °C

The proposed model of microstructural evolution at the zirconia side of ZrO_2/Ti diffusion couple annealed at 1300°C were skematically displayed in Fig. 3. 7. In as hot-pressed zirconia, grain size was about 0.3~0.4 μm in

average [Fig. 3.7(a)]. On heating up to 1300°C, because titanium had a much higher affinity with oxygen than zirconium, ZrO_2 was dramatically reduced to ZrO_{2-x} by titanium and an insignificant grain growth [Fig. 3.7(b)]. During cooling, Zr was excluded from the unstable oxygen-deficient zirconia to the grain boundaries [Fig. 3.7(c)].

3.3.5 Proposed model of phase development at 1550 °C

Figure 3.8 displays schematic diagrams of microstructural evolution of zirconia side in hot-pressed ZrO_2/Ti diffusion couple annealed at 1550°C. In the heating stage, ZrO_{2-x} was initially formed following the fervent oxidatrion–reduction reaction between zirconia and titanium as mentioned above. Then ZrO_{2-x} grains would grow rapidly because the vacancy diffusion was drastically enhanced [Fig. 3.8(b)]. In the cooling stage, the α-Zr segregated on the grains boundaries of ZrO_{2-x} [Fig. 3.8(c)], causing the suppression of grain growth. The microstructure would be varied depending upon the distance from the interface. At the position close to the interface, the oxygen deficient zirconia, with more concentrated oxygen vacancies, would be located in the single c-phase region and experience the displacive diffusionless $c \rightarrow t'$ transformation, resulting in twinned t'-ZrO_{2-x} [Fig. 3.8(d)]. At the position further away the interface, it was believed that the oxygen deficient zirconia, with less oxygen vacancies, was in the (c + t) dual phase region and the lenticular t-ZrO_2 with three variants precipated in the ordered c-ZrO_{2-x} [Fig. 3.8(e)].

3.4 Conclusions

1. The diffusion couple of zirconia and titanium were isothermally annealed at temperatures ranging from 1100° to 1550°C. Three distinct microstructures were found depending upon the annealing temperature.
2. In the zirconia/titanium diffusion couple annealed at 1100°C/6 h, the *t*-ZrO_2 grain did not grow conspicuously and only a trace of oxygen was evolved, yielding *t*-ZrO_{2-x} without α-Zr.
3. After annealing at 1300°C/6 h, more oxygen was evolved from zirconia, resulting in a decreasing O/Zr ratio. The α-Zr was excluded from *t*-ZrO_{2-x}, causing the O/Zr ratio close to 2.
4. When held at 1550°C/6 h, zirconia grains grew rapidly in addition to the vehement oxidation–reduction reaction between zirconia and titanium. The α-Zr was segregated on grain boundaries during cooling by the exsolution of zirconium from ZrO_{2-x}, while twinned *t'*-ZrO_{2-x} or lenticular *t*-ZrO_{2-x}, which was embedded in ordered *c*-ZrO_{2-x}, was found. The ordered *c*-ZrO_{2-x} was identified by the $\frac{1}{5}\{113\}$ superlattice reflections of its electron diffraction patterns.

References

1. G. Economos and W. D. Kingery, "Metal-Ceramic Interactions:II, Mteal Oxide Interfacial Reactions at Elevated Temperatures," *J. Am. Ceram. Soc.*, **36**[12]**,** 403-09 (1953).
2. B. C. Weber, H. J. Garrett, F. A. Mauer, and M. A. Schwartz, "Observations on the Stabilization of Zirconia," *J. Am. Ceram. Soc.*, **39**[6]**,** 197-07 (1956).
3. R. Ruh, "Reaction of Zirconia and Titanium at Elevated Temperatures," *J. Am. Ceram. Soc.*, **46**[7]**,** 301-06 (1963).

4. W. S. Coblenz and R. W. Rice, "Methods of Oxidizing Reduced Ceramics," U. S. Pat. No. 4 568650 (1986).
5. R. W. Rice, *et al.*, "Development and Extension of Partially Stabilized Zirconia Single-Crystal Technology," *Ceram. Eng. Sci. Proc.*, **5**[7-8]**,** 443-74 (1984).
6. S. Moya, R. Moreno, J. Requena, and J. Soria, "Black Color in Partially Zirconia," *J. Am. Ceram. Soc.*, **71**[11]**,** C-479-C-480 (1988).
7. T. Sasaki, *et al.*, "Analytical Study of black colored Y_2O_3-Stabilized Tetragonal Polycrystals," pp. 78-79 in Extended Abstracts of Zirconia '86 Tokyo, Sept. 9-11 (1986).
8. J. H. Park and R. N. Blumental, "Thermodynamic Properties of Nonstoichiometric Yttria-Stabilized Zirconia at Low oxygen Pressures," *J. Am. Ceram. Soc.*, **72**[8]**,** 1485-87 (1989).
9. P. Nicholson, "Influence of reduction on Estimation of the ZrO_2 Tetragonal-Cubic Transformation Temperature," *J. Am. Ceram. Soc.*, **54**[1]**,** 52-53 (1971).
10. R. W. Rice, "Comment on Black Color in Partially Stabilized Zirconia," *J. Am. Ceram. Soc.*, **74**[7]**,** 1745-46 (1991).
11. G. M. Ingo, "Origin of Darkening in 8 wt% Yttria-Zirconia Plasma-Sprayed Thermal Barrier Coatings," *J. Am. Ceram. Soc.*, **74**[2]**,** 381-86 (1991).
12. M. Rühle, N. Claussen, and A. H. Heuer, "Microstructural Studies of Y_2O_3-Containing Tetragonal ZrO_2 Polystals (Y-TZP)"; pp.352-70 in *Advances in Ceramics, Vol. 12, Science and Technology of Zirconia II.* Edited by N. Claussen, M. Rühle and A. H. Heuer. American Ceramic Society, Columbus, OH, 1984
13. C. A. Andersson, J. Greggi, JR., and T. K. Gupta, "Diffusionless Transformations in Zirconia Alloys"; pp.78-85 in *Advances in Ceramics, Vol. 12, Science and Technology of Zirconia II.* Edited by N.

Claussen, M. Rühle and A. H. Heuer. American Ceramic Society, Columbus, OH, 1984

14. T. Sakuma, Y. I. Yoshizawa, and H. Suto, "The Microstructure and Mechanical Properties of Yttria-Stabilize Zirconia Prepared by Arc-Melting," *J. Mater. Sci.*, **20**[10]**,** 2399-407 (1985).
15. A. H. Heuer and M. Rühle, "Phase Transformations in ZrO_2-Containing Ceramic: I, The Instability of c-ZrO_2 and the Resulting Diffusion-Controlled Reactions"; pp. 1-13 in *Advances in Ceramics, Vol. 12, Science and Technology of Zirconia II.* Edited by N. Claussen, M. Rühle and A. H. Heuer. American Ceramic Society, Columbus, OH, 1984
16. V. Lanteri, R. Chaim, and A. H. Heuer, "On the Microstructure Resulting from the Diffusionless Cubic→Tetragonal Transformaion in ZrO_2-Y_2O_3 Alloys," *J. Am. Ceram. Soc.*, **69**[10], C-258-C-261 (1986).
17. A. H. Heuer, "The Displacive Cubic →Tetragonal Transformation in ZrO_2 Alloys," Ac*ta metall.*, **35**[3], 661-66 (1987).
18. V. Lanteri, A. H. Heuer, and T. E. Mitchell, "Tetragonal Phase in the System ZrO_2- Y_2O_3"; pp.118-30 in Ad*vances in Ceramics, Vol. 12, Science and Technology of Zirconia II. E*dited by N. Claussen, M. Rühle and A. H. Heuer. American Ceramic Society, Columbus, OH, 1984
19. A. H. Heuer, V. Lanteri, and A. Dominguez-Rodriguez, "High-Temperature Precipitation Hardening of Y_2O_3 Partially-Stabilized ZrO_2 (Y-PSZ) Single Crystals," *Acta metall.*, **37**[2], 559-67 (1989).
20. N. Ishizawa, *et al.*, "Twin-Related Tetragonal Variants in Yttria Partially Stabilized Zirconia," *J. Am. Ceram. Soc.*, **69**[2], C-18-C-20 (1985).
21. R. Chaim, M. Rühle, and A. H. Heuer, "Microstructural Evolution in a

ZrO_2-12 Wt% Y_2O_3 Ceramic," *J. Am. Ceram. Soc.,* **68**[8], 27-31 (1985).

22. K. F. Lin and C. C. Lin, "Transmission Electron Microscope Investigation of The Interface between Titanium and Zirconia," *J. Am. Ceram. Soc.,* **82**[11], 3179-85 (1999).
23. K. L. Lin and C. C. Lin, "Ti_2ZrO Phases Formed in the Titanium and Zirconia Interface after Reaction at 1550°C," *J. Am. Ceram. Soc.,* **88**[5], 1268–72 (2005).
24. G. Cliff and G. W. Lorimer, "The Quantitative Analysis of Thin Spectimens," *J. Microsc.,* **130**[3], 203-07 (1975).
25. H. Baker, ASM *Handbook, Vol.* 3, Al*loy Phase Diagrams; p*. 2326. ASM International, Metals Park, OH, 1992.
26. H. G. Scoot, "Phase Relationships in the Zirconia-Yttria System," *J. Mater. Sci.,* **10**[9], 1527-35 (1975).
27. R. J. Ackermann, S. P. Garg, and E. G. Rauh, "The lower Phase Boundary of ZrO_{2-x}," *J. Am. Ceram. Soc.,* **61**[5-6], 275-76 (1978).
28. R. J. Ackermann, S. P. Garg, and E. G. Rauh, "High-Temperature Phase Diagram for the System Zr-O," *J. Am. Ceram. Soc.,* **60**[7-8], 341-45 (1977).
29. W. E. Wang and Y. S. Kim, "A Thermodynamic Evaluation of the Titanium-Oxygen System from O/Ti = 0 to 3/2," J. *Nucl. Mater.,* **270**, 242-47 (1999).
30. W. E. Wang and D. R. Olander, "Thermochemistry of the U-O and Zr-O Systems," J. *Am. Ceram. Soc.,* **76**[5], 1242-48 (1993).

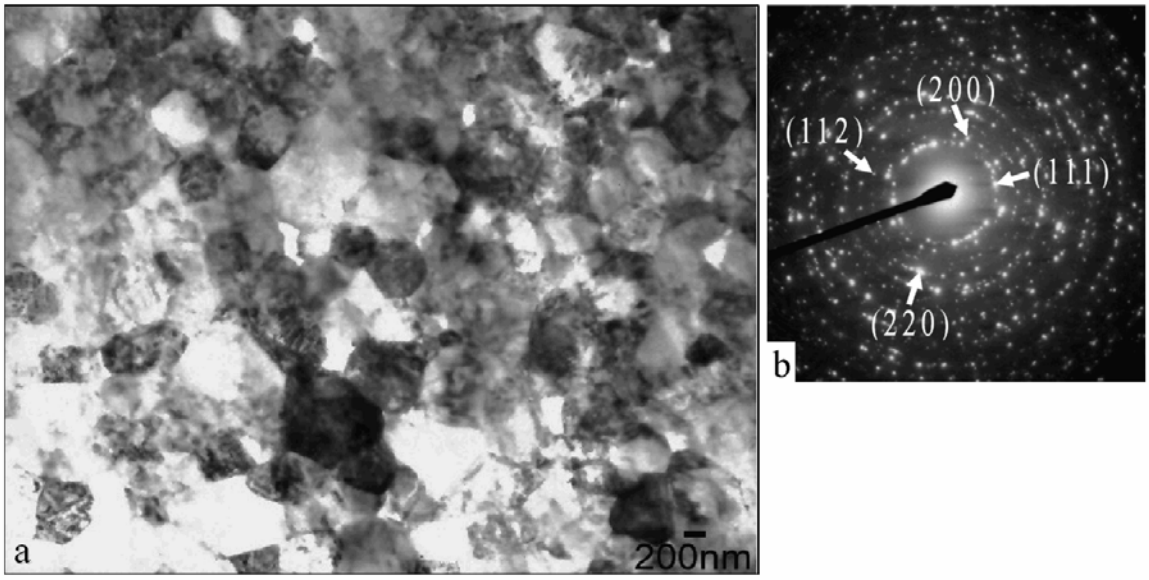

Fig. 3.1 (a) TEM micrograph (bright field image, BFI) of zirconia far away the ZrO_2/Ti interface after reaction at 1100°C/6 h, indicating *t*-ZrO_{2-x} with an average grain size ~0.5 μm; (b) SADP of the *t*-ZrO_{2-x}.

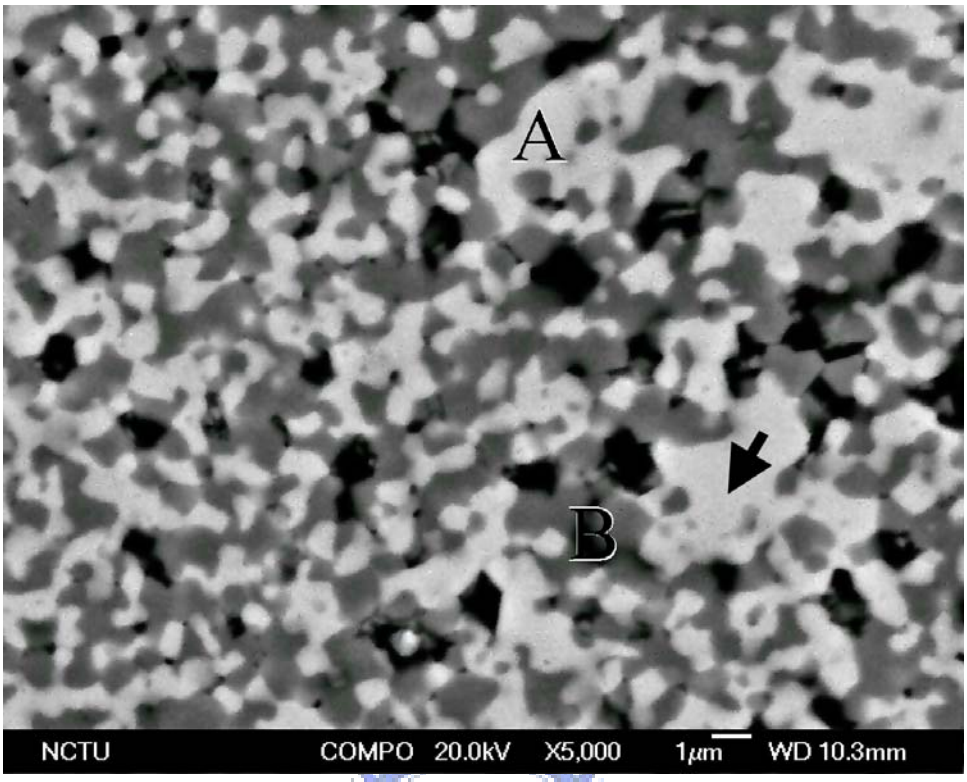

Fig. 3.2 SEM micrograph (backscattered electron image, BEI) of the zirconia side in the ZrO_2/Ti diffusion couple after reaction at 1300°C/6 h, indicating the coexistence of α-Zr (marked as "A") and *t*-ZrO_{2-x}, (marked as "B"). Also shown is the coarsening of α-Zr (arrowed).

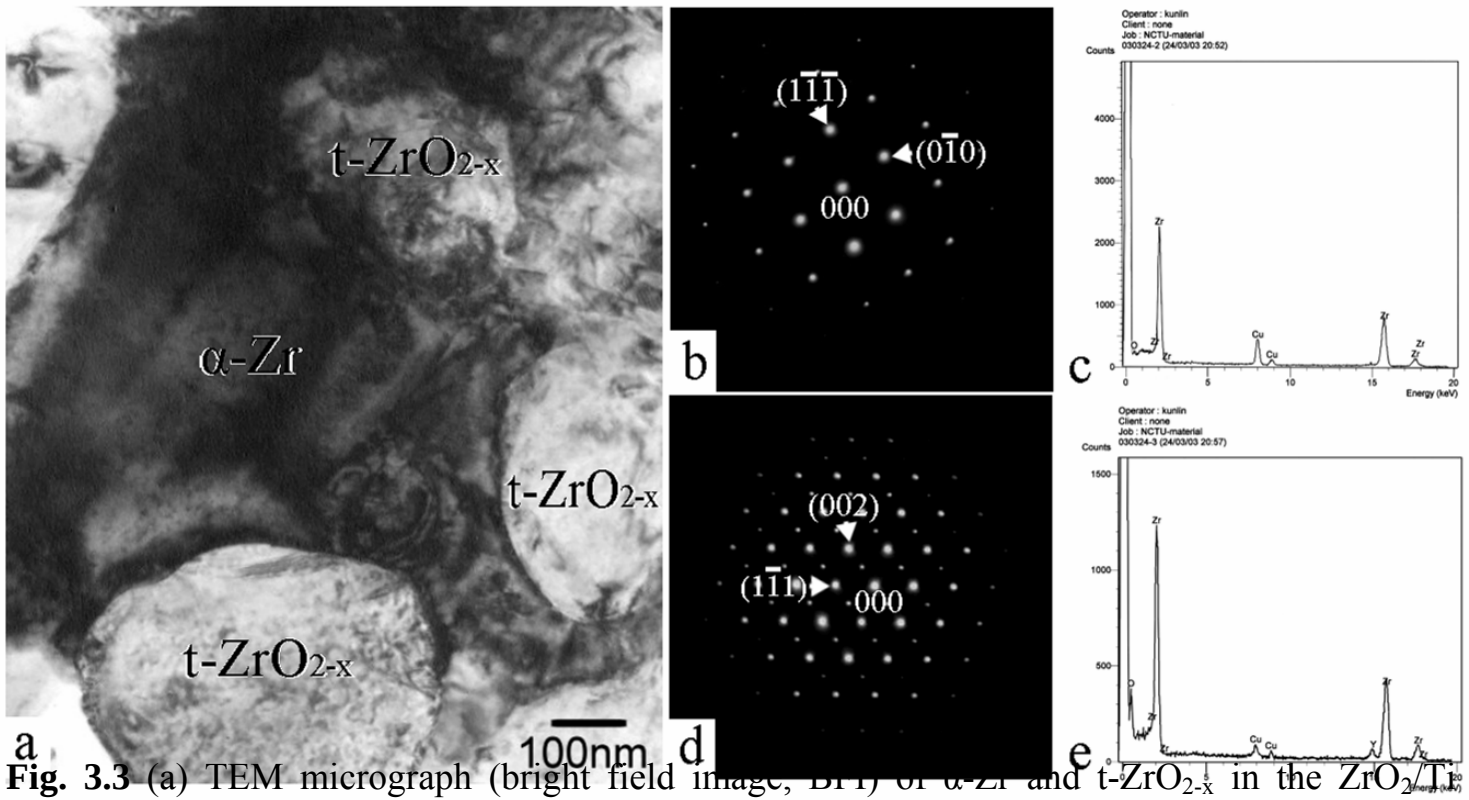

Fig. 3.3 (a) TEM micrograph (bright field image, BFI) of α-Zr and t-ZrO_{2-x} in the ZrO_2/Ti diffusion couple after reaction at 1300°C/6 h; (b) SADP of the α-Zr along the [101] zone axis; (c) EDS of the α-Zr shown in (b); (d) SADP of the *t*-ZrO_{2-x}, along the [110] zone axis; (e) EDS of the *t*-ZrO_{2-x} shown in (d).

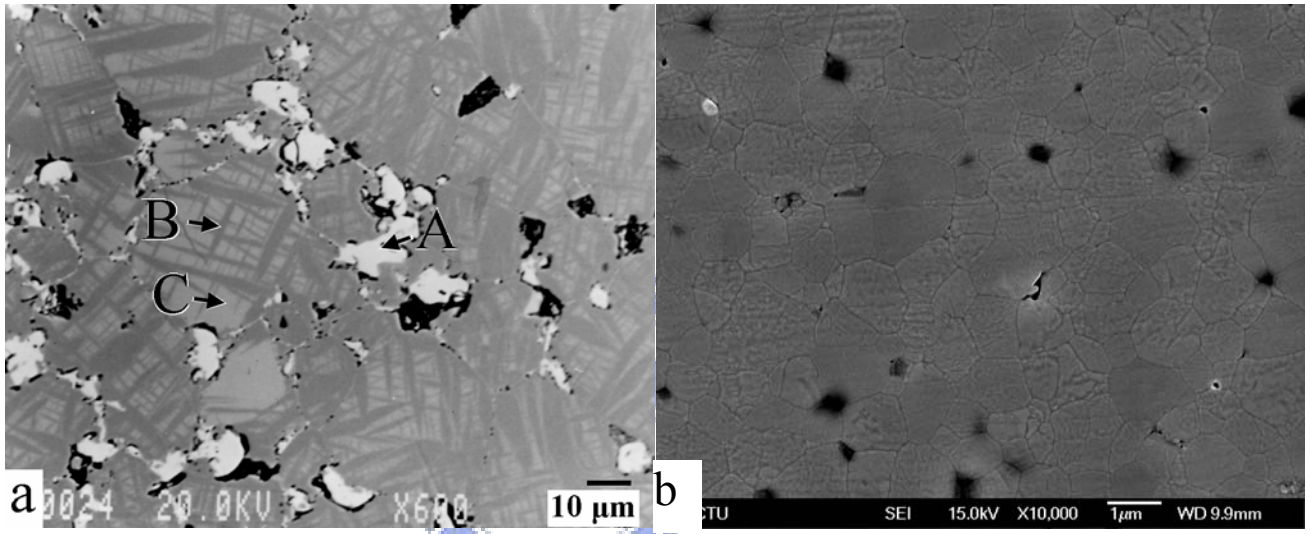

Fig. 3.4 (a) SEM micrograph (backscattered electron image, BEI) of zirconia side in the ZrO_2/Ti diffusion couple after reaction at 1550°C/6 h, indicating the coarsening of intergranular α-Zr (marked as "A") and *t*-ZrO_{2-x} (marked as "B") in the *c*-ZrO_{2-x} matrix (marked as "C"); (b) SEM micrograph (secondary electron image, SEI) of as hot-pressed zirconia after annealing at 1550°C/6 h in Ar.

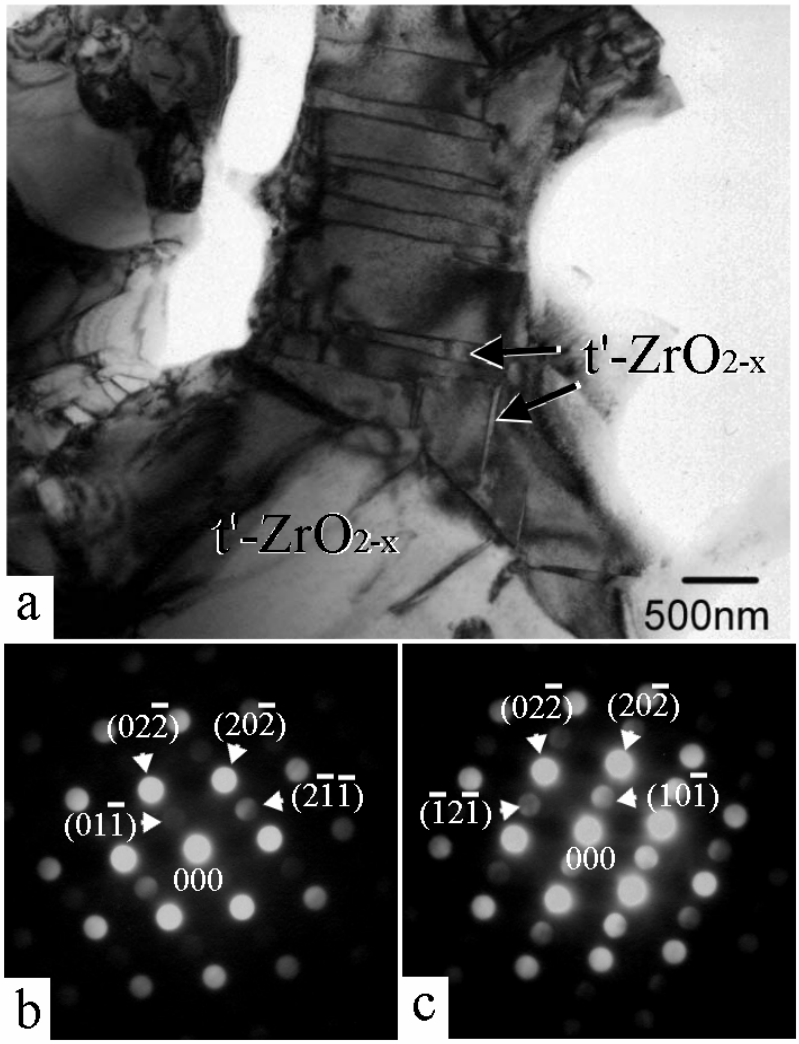

Fig. 3.5 (a) TEM micrograph (bright field image, BFI) of zirconia in the ZrO_2/Ti diffusion couple after reaction at 1550^{o}C/6 h, indicating the twined *t'*-ZrO_{2-x} in *t'*-ZrO_{2-x} matrix; (b) and (c) are microdiffraction patterns from the twined *t'*-ZrO_{2-x} and the *t'*-ZrO_{2-x} matrix along the zone axes of [111], respectively.

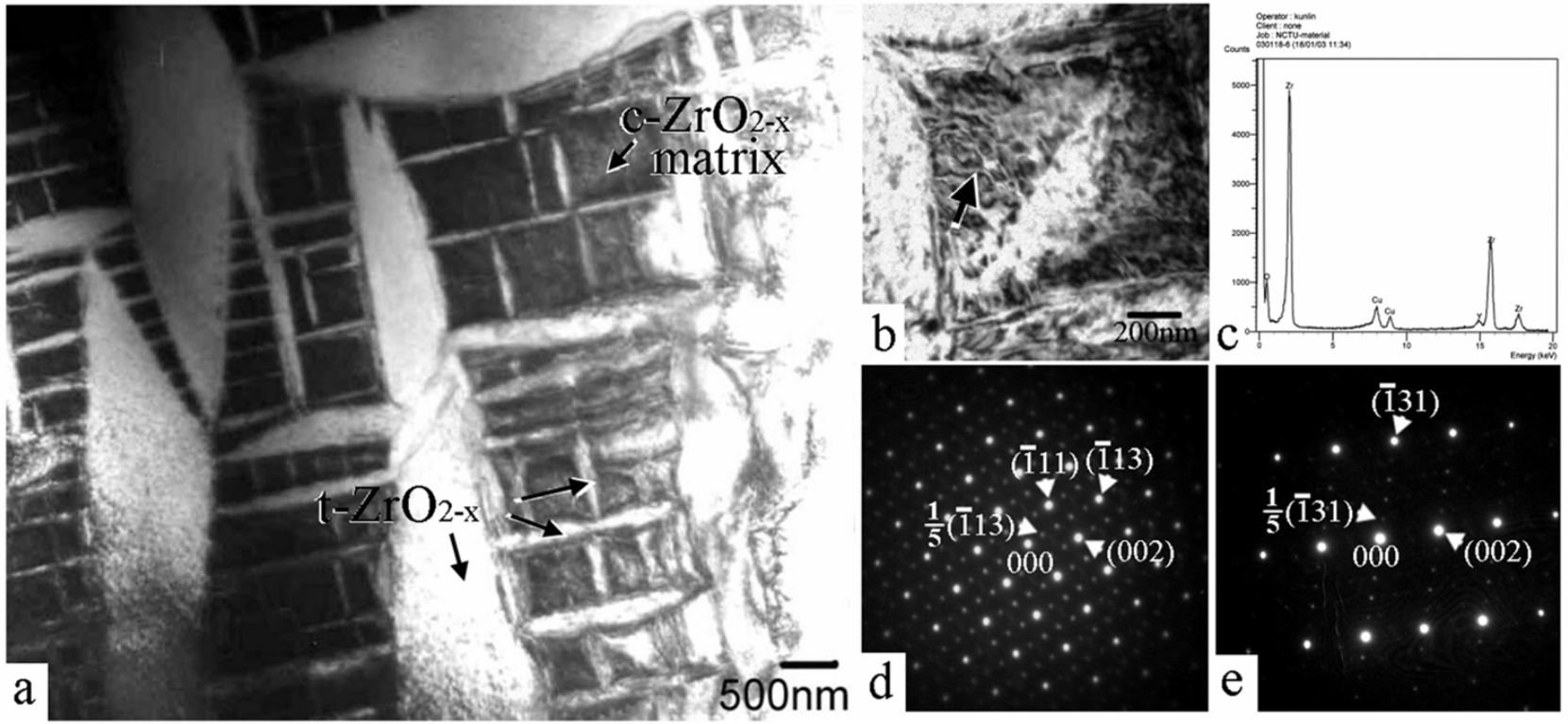

Fig. 3.6 (a) TEM micrograph (bright field image, BFI) of zirconia in the ZrO_2/Ti diffusion couple after reaction at 1550°C/6 h, displaying {100} type of variants of the lenticular *t*-ZrO_{2-x} in *c*-ZrO_{2-x} matrix; (b) A magnified image of the *c*-ZrO_{2-x} matrix in (a), showing the ordered structure; (c) EDS of the ordered *c*-ZrO_{2-x}; (d) and (e) are SADP's of the ordered *c*-ZrO_{2-x} matrix with zone axis being [110] and [310], respectively.

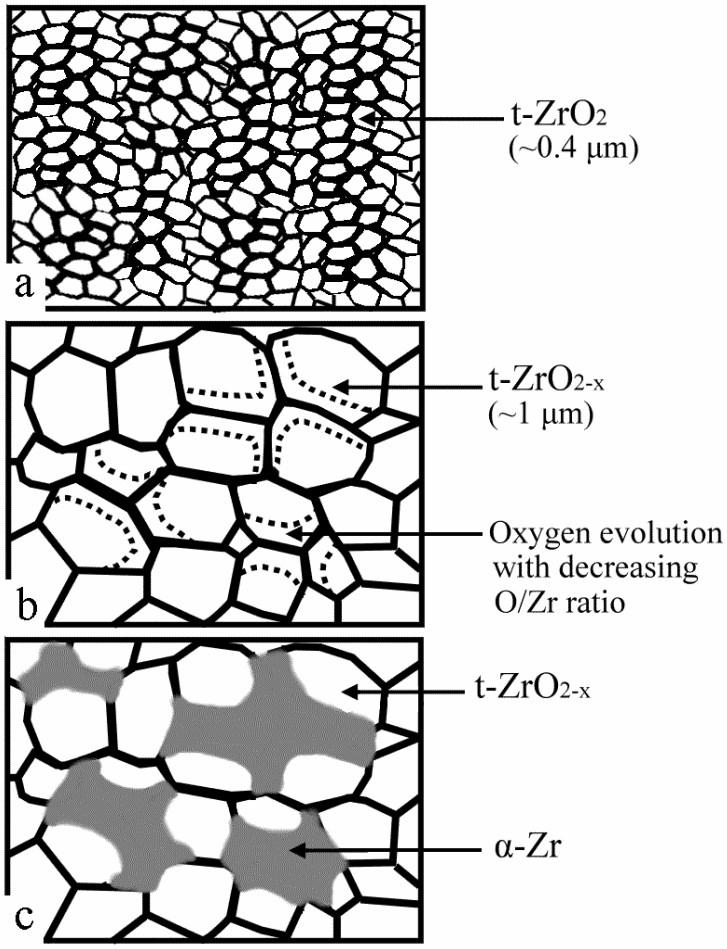

Fig. 3.7 Schematic diagrams showing the microstructural evolution of the zirconia side in the ZrO_2/ Ti diffusion couple annealed at 1300^{o}C/6 h. (a) as hot-pressed; (b) grain growth on heating to 1300^{o}C; (c) exclusion of α-Zr from ZrO_{2-x} during cooling.

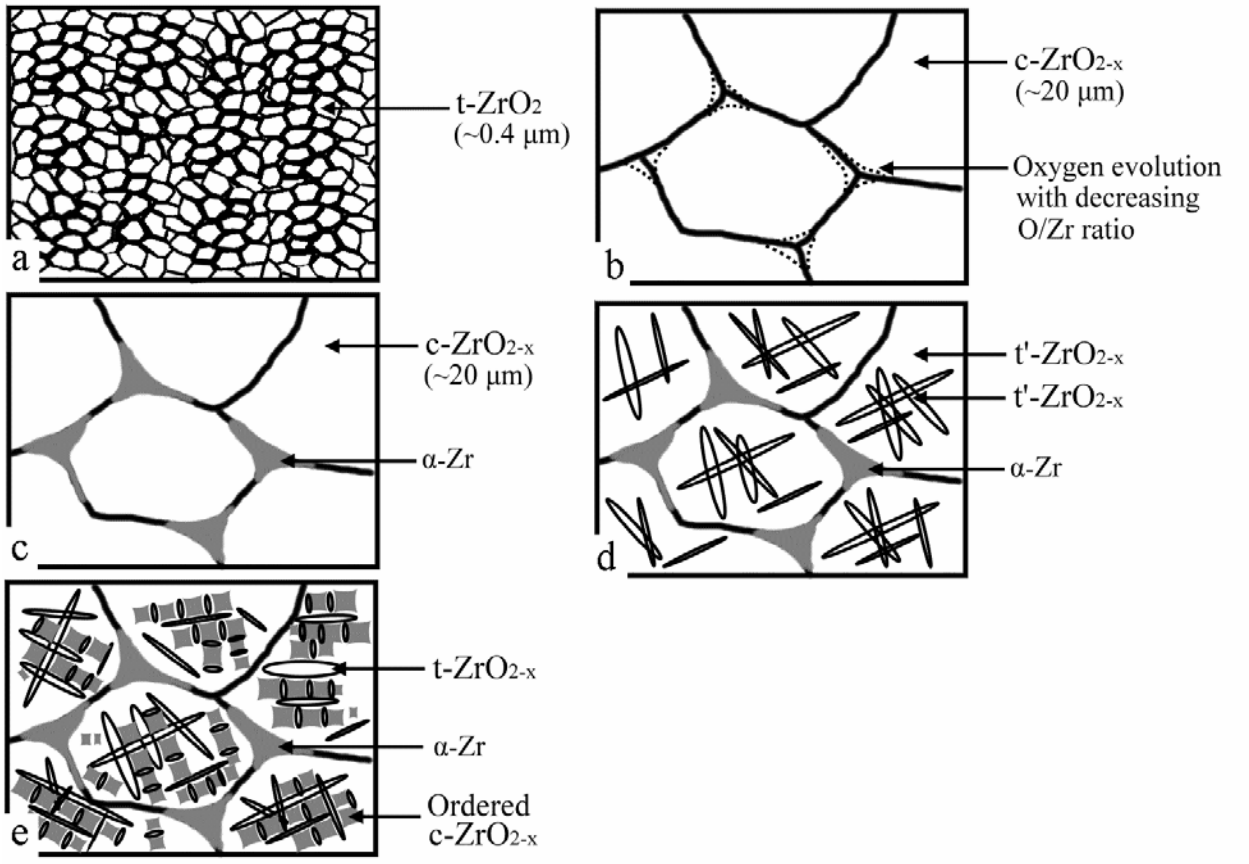

Fig. 3.8 Schematic diagrams showing the microstructural evolution of the zirconia side in ZrO_2/Ti diffusion couple annealed at 1550°C/6 h. (a) as hot-pressed; (b) apparent grain growth on heating to 1550°C; (c) exclusion of α-Zr during cooling; (d) formation of twined *t'*-ZrO_2; (e) the formation of lenticular *t*-ZrO_2 and ordered *c*-ZrO_{2-x} during cooling.